JOURNAL OF AIRCRAFT
Vol. 38, No. 6, November–December 2001

# Perturbations of a Delta Wing: Control of Vortex Breakdown and Buffeting

M. Özgören,* B. Sahin,* and D. Rockwell†
*Lehigh University, Bethlehem, Pennsylvania 18015*

**A delta wing is subjected to small-amplitude perturbations over a range of periods, to simulate leading-edge control concepts. Substantial modifications of the instantaneous and averaged structure of the leading-edge vortex are attainable, both with and without a downstream impingement plate. The features of the vortex response are characterized using a technique of high-image-density particle image velocimetry. The location of the onset of vortex breakdown can either be advanced or retarded, and the attendant changes in vortex structure are interpreted in the context of buffeting of the impingement plate. Comparison of the vortex structure with and without deployment of the plate shows a dramatic influence of the plate.**

## Nomenclature

| | | |
|---|---|---|
| $C$ | = | chord of delta wing, mm |
| $D'_v$ | = | characteristic vortex diameter, mm |
| $f_e$ | = | perturbation frequency of the wing, Hz |
| $f_0$ | = | frequency of vortex breakdown, Hz |
| $L$ | = | distance between trailing edge of the delta wing and leading edge of the plate |
| $L_p$ | = | length of the plate, mm |
| $M$ | = | magnification |
| $N$ | = | number of samples |
| $Re$ | = | Reynolds number, $U_\infty C/\nu$ |
| $T$ | = | total time of sample, s |
| $T_e$ | = | period of wing perturbation, s |
| $T_0$ | = | period of inherent (undisturbed) vortex breakdown, s |
| $U_{\text{ref}}$ | = | reference velocity, mm/s |
| $U_\infty$ | = | freestream velocity, mm/s |
| $V$ | = | total velocity, mm/s |
| $\langle V \rangle$ | = | averaged velocity, mm/s |
| $v$ | = | transverse velocity component, mm/s |
| $v_{\text{rms}}$ | = | root mean square of transverse velocity fluctuations, mm/s |
| $W_p$ | = | width of the plate, mm |
| $X_b^*$ | = | vortex breakdown location in presence of wing perturbation, mm |
| $(X_b^*)_0$ | = | vortex breakdown location for stationary wing, mm |
| $\alpha$ | = | angle of attack of delta wing, deg |
| $\alpha(t)$ | = | dynamic angle of attack of delta wing, deg |
| $\alpha_0$ | = | amplitude of wing perturbation, deg |
| $\bar{\alpha}$ | = | mean angle of attack, deg |
| $\Delta\omega$ | = | incremental values of vorticity, 1/s |
| $\Lambda$ | = | sweep angle of delta wing, deg |
| $\nu$ | = | kinematic viscosity, mm$^2$/s |
| $\omega$ | = | vorticity, 1/s |
| $\langle\omega\rangle$ | = | averaged vorticity, 1/s |
| $\omega_e$ | = | angular velocity of wing perturbation, rad/s |

Received 2 April 2000; revision received 12 June 2001; accepted for publication 13 June 2001. 

*Visiting Scientist, Department of Mechanical Engineering and Mechanics, 354 Packard Laboratory, 19 Memorial Drive West; Professor, Department of Mechanical Engineering, Cukurova University, Balcali 01330 Adana, Turkey.

†Paul B. Reinhold Professor, Department of Mechanical Engineering and Mechanics, 354 Packard Laboratory, 19 Memorial Drive West.

## I. Introduction

### Buffeting of Tails and Plates

INTERACTION of vortices with aerodynamic surfaces, such as tails and plates, induces unsteady surface loading, often referred to as buffeting. Lee[1] gives an extensive overview of this area of unsteady aerodynamics. Wolfe et al.[2] correlated data from a diverse set of experiments, extending over a wide range of Reynolds and Mach number. The emphasis was on correlations of the predominant frequency of buffeting. Measurement of spectra of pressure fluctuations on either a tail or a plate are reported in the works of Washburn et al.,[3] Bean and Wood,[4] Canbazoglu et al.,[5] and Wolfe et al.[6] Considerable effort has focused on the buffeting of tails (fins) of F-series aircraft, with emphasis on the surface pressure loading and acceleration response. For the case of a model F-15 aircraft, Triplett[7] determined the fluctuations on the surface of the tail. Studies of model F-18 aircraft, which primarily focused on the surface pressure spectra on tails (fins), include the works of Wentz,[8] Ferman et al.,[9] Zimmerman et al.,[10] Shah,[11] Lee and Tang,[12] Martin and Thompson,[13] and Lee et al.[14] Similar types of measurements on the fin of a model F-22 aircraft were undertaken by Moses and Huttsell.[15] Luber et al.[16] addressed the role of dynamic loads on the design of aircraft. Use of active control techniques applied directly to the surface of a fin can effectively attenuate the buffet response, as demonstrated by Ashley et al.[17]

Of course, the origin of buffeting of any aerodynamic surface is the unsteady flow adjacent to it. For the case of the tail buffet problem, knowledge of the physical structure of the vortex incident upon, and its interaction with, the tail is of central importance. Breitsamter and Laschka[18–20] used a hot-wire anemometer technique to map the fluctuating flow pattern associated with vortex breakdown in absence of a tail; they employed these data to calculate the surface loading. Beutner et al.[21] used planar Doppler velocimetry to measure the root-mean-square distributions of the unsteady flow parameters associated with impingement of a vortex upon a fin. A sequence of investigations, which employed high-image-density particle image velocimetry (PIV) involves the works of Mayori and Rockwell[22] and Wolfe et al.[6] to determine the distortion of vortex breakdown during its interaction with a thin flat plate and the investigation of Canbazoglu et al.[5,23] to define the instantaneous patterns of vortex distortion during its interaction with a tail. Related numerical investigations are not summarized here; they are provided by Rockwell.[24]

The issue arises as to whether control of vortices from the leading edges of a delta wing can provide modification of the flowfield associated with buffet loading of an aerodynamic surface such as a wing or tail. In the sections that follow, various vortex control techniques are described. Then the potential for modification of the buffet flowfield via vortex control is addressed. Finally, these previous

related investigations form the basis for defining the unresolved issues for the present investigation: the detailed structure of controlled vortices and their interaction with a simulated tail, that is, a plate.

#### Vortex Control by Unsteady Flap or Unsteady Freestream

Control by a flap undergoing relatively large-amplitude transient displacement or, alternatively, periodic oscillation, is addressed by Spedding et al.[25] and Karagounis et al.[26] Analogous to the approach of oscillating a flap or an entire wing is perturbation of the freestream past a stationary wing, as undertaken by Gursul et al.[27]

#### Vortex Control by Axial or Tangential Blowing/Suction

Either steady or unsteady fluid injection has been employed at the leading edge of a delta wing. Control approaches in this category are reviewed by Rockwell.[28] Steady control in the form of a single jet oriented along the axis of the vortex was addressed by Shih et al.[29] and Visser et al.,[30] as well as by investigators cited therein. A major consequence of this approach is an increase in length of the vortex core to the onset of vortex breakdown. The effectiveness of steady tangential blowing was shown in the investigation of Wood and Roberts,[31] followed by a series of investigations, including that of Celik and Roberts.[32] Flow visualization showed that blowing can effectively alter the structure of the leading-edge vortex at high angle of attack.

Regarding unsteady control approaches, Gad-el-Hak and Blackwelder[33] applied unsteady blowing–suction in a direction normal to a relatively thin leading edge and observed alteration of the initially formed small-scale vortices from the leading edge. Both steady and unsteady tangential blowing and suction at the leading edge of a delta wing were addressed by Gu et al.[34] They show that the onset of vortex breakdown could be displaced a substantial distance downstream by use of these approaches. In a related numerical simulation, Findlay et al.[35] showed the effect of a steady slit jet oriented normal to the leading edge; changes in both the location and strength of the leading-edge vortex were attained.

#### Control of Vortex–Tail Interaction by Tangential Blowing

The foregoing investigations address techniques for controlling the structure of vortices. If the onset and structure of vortex breakdown can be altered, it will have important implications for buffet of, for example, a wing surface, as well as an aerodynamic appendage or a tail located in the path of the vortex. Of all of the aforementioned control approaches, only tangential blowing concepts have been employed to modify tail buffeting. Tangential blowing at the leading edges of a delta wing can alter the buffet loading of tails, as demonstrated by Bean and Wood.[4] Moreover, Huttsell et al.[36] describe a range of investigations involving tangential blowing at a number of locations on an actual model of an aircraft, with the aim of altering the buffet-induced loading.

#### Vortex Control by Insertion of a Body or Edge

A type of vortex control not addressed in the preceding sections involves the inherent upstream influence from a body or surface located within the vortex. Even relatively small geometries can have a significant effect. Reynolds and Abtahi[37] demonstrated that insertion of a probe in a leading-edge vortex could substantially alter the location of vortex breakdown. Furthermore, Gursul and Yang[38] showed that deployment of a control cylinder could cause the early onset of breakdown of a leading-edge vortex. Akilli et al.[39] have revealed that a small control wire, having a diameter two orders of magnitude smaller than the vortex diameter, can substantially alter the onset of breakdown. At the other extreme, if a relatively large tail is placed in the path of a vortex and subjected to controlled perturbations, the vortex–tail interaction exhibits a coupled behavior, as demonstrated by Gursul and Xie.[40] Sahin et al.[41] have shown a conceptually similar effect for vortex interaction with an oscillating plate. They showed that vortex breakdown incident upon an oscillating plate can show markedly different patterns of vortex structure, depending on the ratio of the perturbation frequency to the inherent frequency of vortex breakdown.

#### Unresolved Issues

The overall objective of the present investigation is to simulate the effect of unsteady leading-edge control, and its consequence for buffeting of surfaces located within or adjacent to the vortex. Examples of control concepts include unsteady blowing, suction, flaps, microflaps and MEMS (microelectromechanical systems) actuators. All of these approaches alter the vorticity originating from the separation line along the leading edge. Perturbations of the wing, and thereby its leading edges, will alter the vorticity generation from the separation line in a fashion analogous to the aforementioned control concepts. When the wing is subjected to perturbations over a range of frequencies, it will be possible to observe the response of the vortex to an applied perturbation.

The major unresolved issues pertaining to the theme of the present investigation are 1) the effect of small-amplitude perturbations at the leading edges of a swept wing on the occurrence of vortex breakdown, 2) the sensitivity of vortex breakdown to the value of perturbation frequency, relative to the inherent frequency of vortex breakdown, and 3) the consequence of this altered vortex structure on the velocity fluctuations in the vicinity of the plate, which are central to models of buffet loading. The response of the vortex to applied perturbations should also be considered in absence of the impingement plate. Comparison with the foregoing results would show if the plate in the vortex influences the effectiveness of the perturbations. This investigation addresses these issues using a technique of high-image-density PIV, which allows characterization of the instantaneous and averaged patterns of vorticity and velocity.

## II. Experimental System and Techniques

All experiments were performed in a large-scale water channel having a width of 927 mm and a height of 610 mm. The water height in the channel was maintained constant at a value of 559 mm. The delta wing system indicated in the schematic of Fig. 1 was mounted in this test section. The wing–plate system is similar to that employed by Sahin et al.[41] for which the wing was maintained stationary and the impingement plate was subjected to controlled oscillations. The delta wing has a sweep angle of $\Lambda = 75$ deg, a chord $C = 222$ mm, and a thickness of 3.2 mm. The bevel angle of the wing on the windward side was 34 deg. The plate had a length of $L_p = 162$ mm

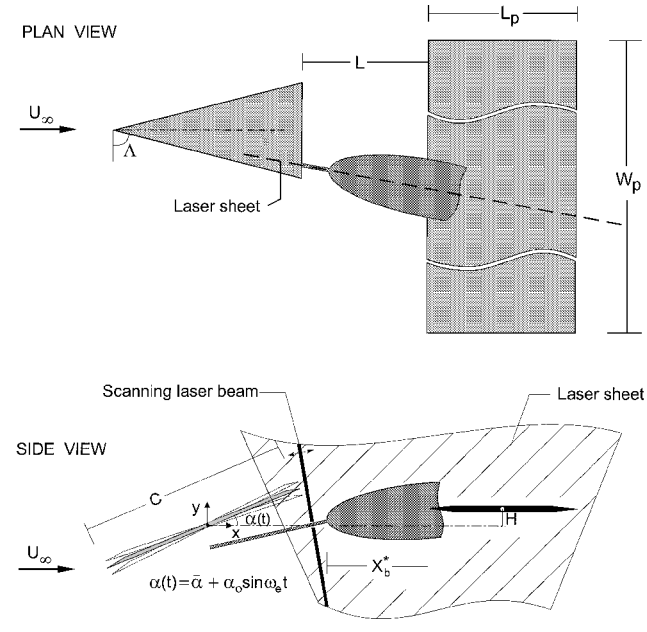


**Fig. 1 Schematics of delta wing subjected to small-amplitude perturbations about its midchord, which changes the structure of the leading-edge vortex and its breakdown, thereby altering the unsteady nature of vortex impingement on the plate.**

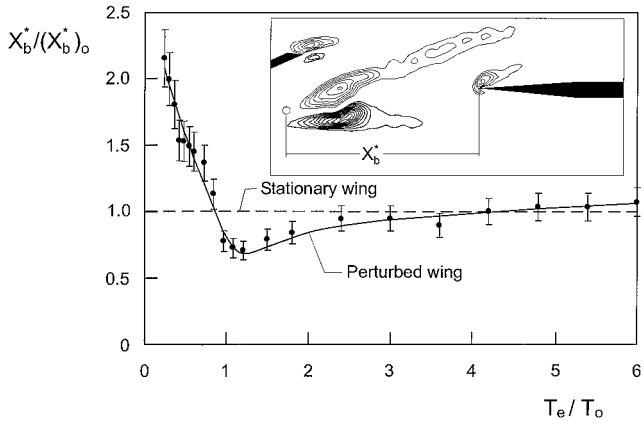


**Fig. 2 Time-averaged location $X_b^*$ of onset of vortex breakdown due to small-amplitude perturbation of delta wing, normalized by the value $(X_b^*)_0$ corresponding to the stationary wing.**

and a thickness $t_p = 6.35$ mm; its leading and trailing edges were beveled at angles 5 and 12 deg, respectively. The distance between the trailing edge of the delta wing and the leading edge of the plate was maintained at $L = 73$ mm. The wing was subjected to small-amplitude controlled perturbations of the form $\alpha(t) = \bar{\alpha} + \alpha_0 \sin \omega_e t$, in which $\omega_e = 2\pi f_e$. The period $T_e = 2\pi/\omega_e$ was varied over the interval $0.5 \le T_e \le 2$ s, relative to the period $T_0 = 1.6$ s of the inherent nonperturbed spiral ($n = 1$) mode of vortex breakdown. Values of $T_0$ were determined from time records of dye visualization of the periodic, three-dimensional vortex pattern, at a location immediately after the onset of vortex breakdown. Over 100 oscillation cycles were averaged to obtain the value of $T_0$.

The mean angle of attack of the wing was maintained constant at $\bar{\alpha} = 24$ deg. The amplitude of the wing perturbation was $\alpha_0 = 1$ deg. Throughout the experiments, the value of free-stream velocity was $U_\infty = 48$ mm/s. The Reynolds number, based on chord $C$ of the wing, was $Re = 1.07 \times 10^4$.

A technique of high-image-density PIV allowed determination of the instantaneous flow patterns over a plane passing through the centerline of the vortex. This technique is based on a laser-scanning concept, as described by Rockwell et al.[42] The schematic of Fig. 1 shows the extent of the laser sheet generated by the scanning laser

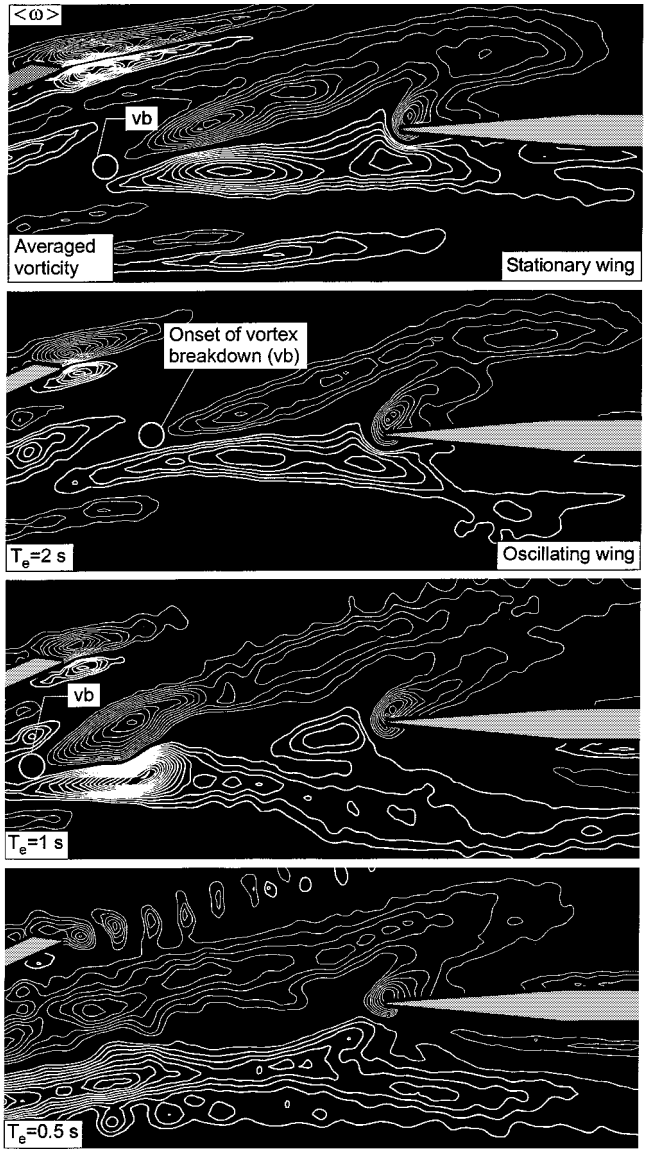


**Fig. 3a Contours of averaged vorticity $\langle\omega\rangle$ for the stationary wing and wing subjected to small-amplitude perturbation at designated period $T_e$ in presence of the impingement plate, relative to the period $T_0 = 1.6$ s of the inherent instability of vortex breakdown.**

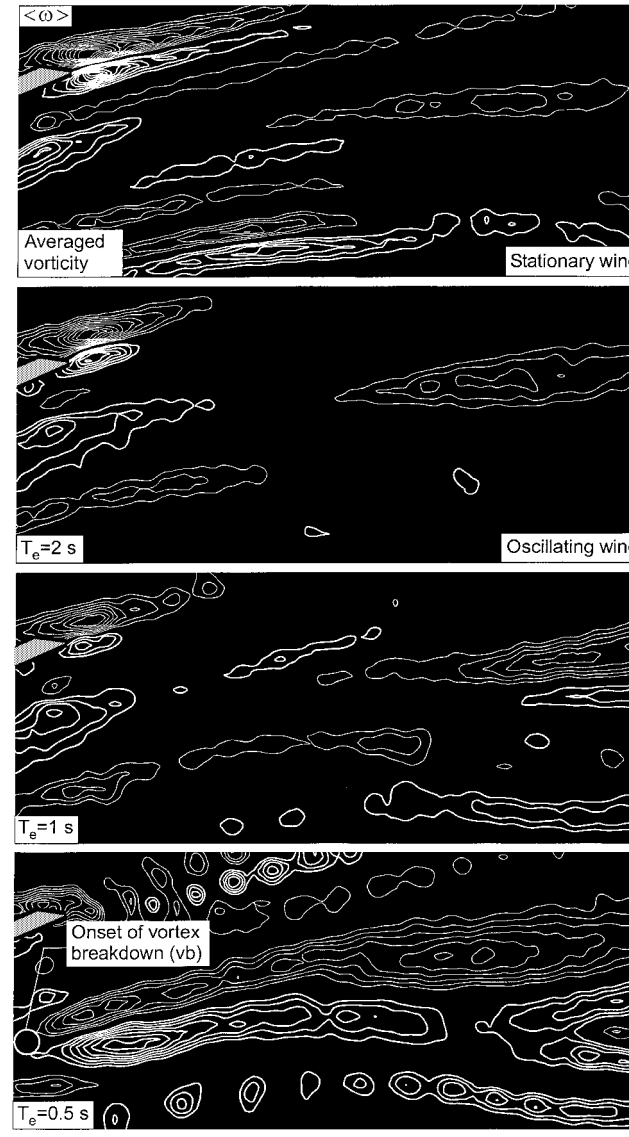


**Fig. 3b Contours of averaged vorticity $\langle\omega\rangle$ for the stationary wing and wing subjected to small-amplitude perturbation at designated period $T_e$ in absence of the impingement plate, relative to the period $T_0 = 1.6$ s of the inherent instability of vortex breakdown.**

beam. The sheet was oriented such that it passed through the center of the vortex, including the region of vortex breakdown. The central feature of this scanning laser beam technique is impingement of the laser beam on a rotating polygonal mirror having eight facets. At the selected value of freestream velocity, the most effective scanning frequency of this beam was 75 Hz. To optimize the quality of the laser sheet generated using this approach, as well as to minimize the thickness of the sheet, which was approximately 1 mm, the laser beam was transmitted through a sequence of focusing optics before its impingement on the rotating polygonal mirror.

Effective seeding of the flow with small particles is essential to obtain high-quality images for the technique of high-image-density PIV. This seeding was accomplished by use of metallic-coated, hollow plastic spheres, which had a diameter of 14 $\mu$m.

Image acquisition involved a Canon EOS-1 camera. It effectively captured the multiply exposed particle images generated by successive scans of the laser beam. The camera was operated at a shutter speed of 1/15 s and a value of $\mathcal{F}$-stop of $\mathcal{F} = 5$. The desired field of view of the laser sheet required a camera lens having a magnification of $M = 1{:}4.24$. Because the instantaneous flow patterns of vortex breakdown involve regions of reverse flow, it was necessary to deploy an oscillating bias mirror ahead of the camera lens to avoid issues associated with directional ambiguity. High-resolution 35-mm film (300 lines/mm) was employed to record the particle images. These negatives of the particle image patterns were then digitized with a resolution of 125 pixels/mm. To evaluate the velocity field, a single-frame, cross-correlation technique was applied to the patterns of particle images. The most effective size of the interrogation window was 90 × 90 pixels. A 50% overlap was maintained, in accord with the Nyquist criterion. Approximately 50 particle images were located within the interrogation window, thereby ensuring that the criterion of high image density was exceeded. With the aforementioned value of magnification factor, the effective grid size in the physical plane of the laser sheet was 1.53 × 1.53 mm. During acquisition of the images of the flow pattern, the framing rate of the motor-driven Canon EOS-1 camera was 5.55 frames/s. A Gaussian filter with a factor of $p = 1.3$ was applied to the calculated velocity field. No additional filtering of the data was carried out. The total number of velocity vectors was 5734. The field of view of the images is 141 × 62 mm.

Representations of the flow pattern, to be described subsequently, involve not only instantaneous images of velocity and vorticity, but also averaged representation of these quantities, as defined by the following equations:

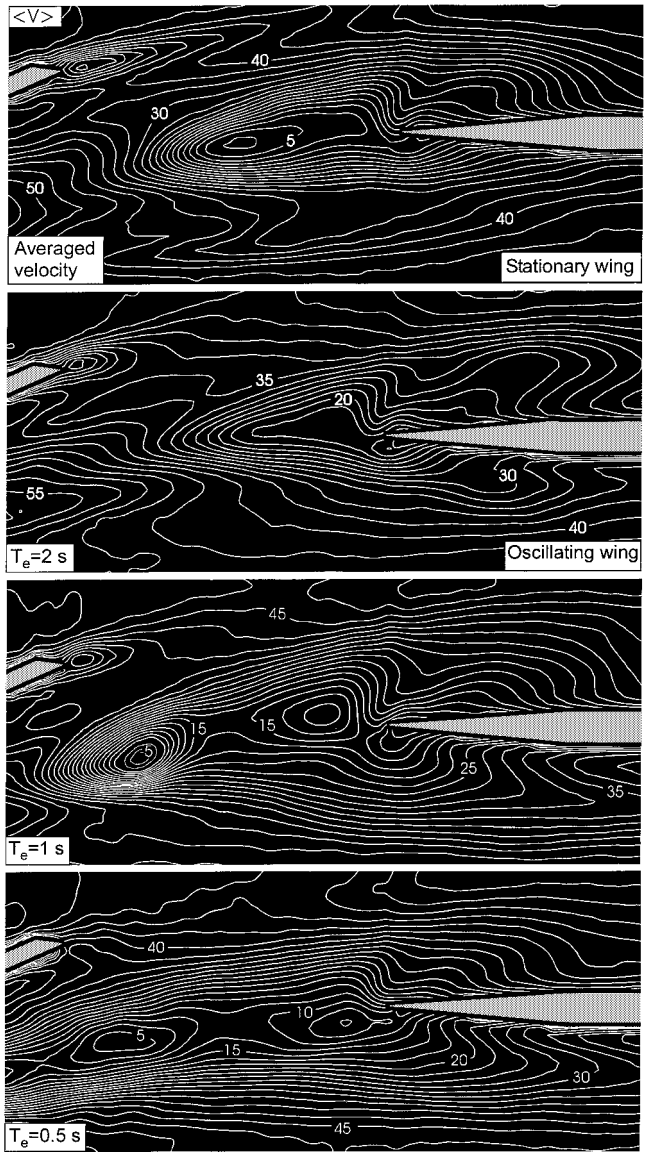


**Fig. 4a Contours of constant averaged velocity $\langle V \rangle$ for the case of the stationary delta wing and wing subjected to small-amplitude perturbation at designated period $T_e$, relative to period $T_0 = 1.6$ s of inherent instability of vortex breakdown in presence of the impingement plate.**

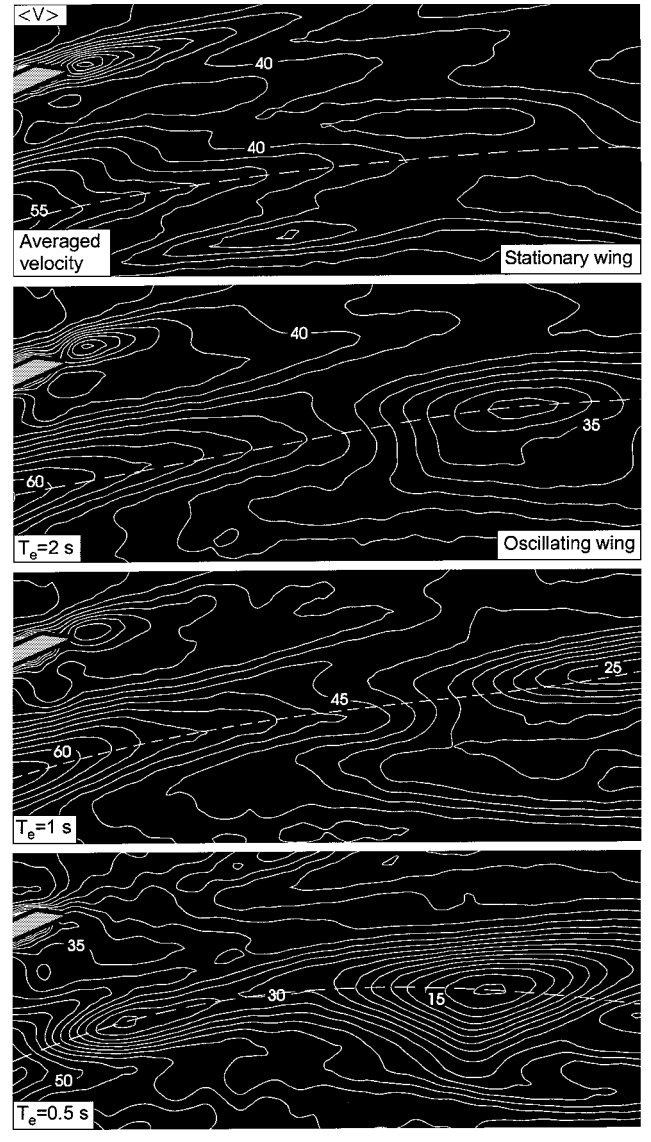


**Fig. 4b Contours of constant averaged velocity $\langle V \rangle$ for the case of stationary delta wing and wing subjected to small-amplitude perturbation at designated period $T_e$, relative to period $T_0 = 1.6$ s of inherent instability of vortex breakdown in absence of the impingement plate.**

$$\langle V \rangle = \frac{1}{N} \sum_{n=1}^{N} V_n(x, y) \tag{1a}$$

$$\langle \omega \rangle = \frac{1}{N} \sum_{n=1}^{N} \omega_n(x, y) \tag{1b}$$

$$v_{\text{rms}} = \left\{ \frac{1}{N} \sum_{n=1}^{N} [v_n(x, y) - \langle v(x, y) \rangle]^2 \right\}^{\frac{1}{2}} \tag{1c}$$

In these equations, $N$ is the total number of PIV images. Averaged representations were obtained by averaging a total of 36 images.

## III. Time-Averaged Structure of Vortex

### Averaged Location of Vortex Breakdown

An overview of the consequence of wing perturbations on the averaged location of vortex breakdown in presence of the impingement plate is shown in Fig. 2. The onset of breakdown is indicated as $X_b^*$, relative to its value $(X_b^*)_0$ for the case of the stationary wing. This value of $X_b^*/(X_b^*)_0$ as a function of $T_e/T_0$, in which $T_e$ is the period of the wing perturbation and $T_0$ is the inherent period of vortex breakdown. As indicated in the inset of the schematic of Fig. 2, the onset of vortex breakdown $X_b^*$ is taken to correspond to the leading edges of the vorticity concentrations arising from the initial portion of the breakdown bubble. In Fig. 2, the vertical bars at each data point correspond to the extreme values of $X_b^*$ determined during the course of data acquisition. The filled circular symbols represent the averaged values. In Fig. 2 the mean and perturbation angle of attack are $\bar{\alpha} = 24$ deg and $\alpha_0 = 1$ deg. The period of natural instability of the vortex breakdown is $T_0 = 1.6$ s.

It is evident that retardation of the onset of vortex breakdown occurs over a significant range of excitation period of the wing, extending approximately from $0.9 < T_e/T_0 < 4.3$. Maximum retardation occurs at a ratio of approximately $T_e/T_0 = 1.2$, which corresponds to a value of $f_e C/U_\infty = 7.4$. On the other hand, a rather dramatic advancement of the onset of vortex breakdown occurs at low values of $T_e/T_0$, with particularly large values attained in the vicinity of $T_e/T_0 = 0.2$. These alterations of the onset of vortex breakdown are accompanied by substantial changes in the averaged and instantaneous structure of the breakdown process, as described in the following.

### Patterns of Averaged Vorticity in Presence and Absence of Impingement Plate

Averaged contours of vorticity $\langle \omega \rangle$ are shown in Fig. 3a for the case where the impingement plate is deployed immediately downstream of the trailing edge of the delta wing. Images are exhibited for the case of the stationary wing, as well as the wing subjected to small-amplitude perturbations of angle of attack at period $T_e$. In Figs. 3a and 3b, thick and thin lines represent positive and negative vorticity, respectively. Minimum and incremental values of vorticity are $\omega_{\min} = \pm 1\ \text{s}^{-1}$ and $\Delta_\omega = 0.5\ \text{s}^{-1}$. Nominal angle of attack of the delta wing is $\bar{\alpha} = 24$ deg and amplitude of the perturbation angle of attack is $\alpha_0 = 1$ deg. When the wing is perturbed at $T_e = 2$ s, the onset of vortex breakdown moves downstream, and the peak vorticity level along the edge of the separation bubble is significantly decreased. On the other hand, at $T_e = 1$ s, the onset of vortex breakdown is

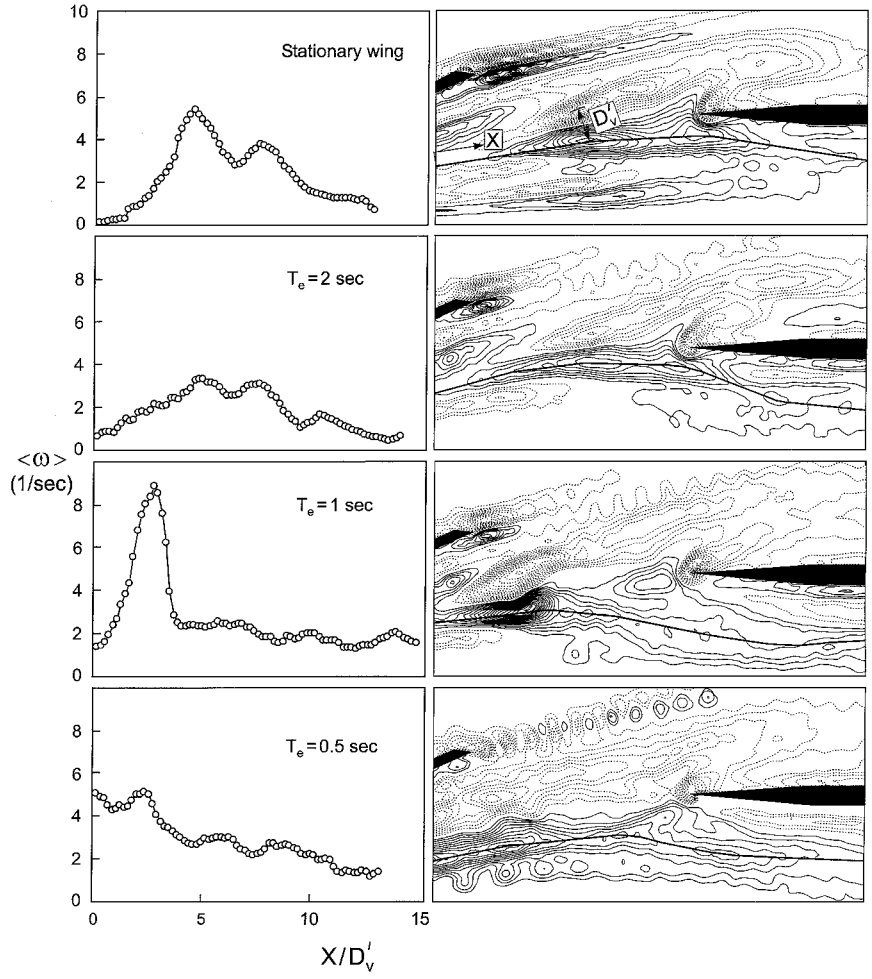


**Fig. 5 Variation of averaged vorticity $\langle \omega \rangle$ along a line corresponding to maximum positive vorticity for the case of a stationary wing and wing subjected to perturbation and angle of attack at period $T_e$, relative to the period $T_0 = 1.6$ s of the inherent instability of vortex breakdown.**

advanced in the upstream direction, and the pattern of vorticity in the leading portion of the bubble is characterized by a high level of vorticity concentration. Farther downstream along the edges of the vortex breakdown bubble, the peak values of vorticity are, however, dramatically lower than those immediately following the onset of vortex breakdown. Finally, for the case $T_e = 0.5$ s, the onset of vortex breakdown is advanced well upstream of the location of the left boundary of the image; in fact, independent dye visualization shows that it occurs at a location of approximately $0.85C$ measured from the trailing edge of the delta wing, in which $C$ is the wing chord (Fig. 1). In this case, even though the onset of breakdown occurs relatively early, significant levels of vorticity are indeed evident along the edges of the breakdown bubble at axial locations in the vicinity of the leading edge of the plate.

To determine the effect of deployment of the impingement plate, the same experiments were executed in absence of a plate. The averaged vorticity contours are shown in Fig. 3b. For the case of the stationary wing, represented by the top image, only very low-level vorticity contours are apparent in the central region of the vortex, and no indication of vortex breakdown is evident; in fact, independent dye visualization showed vortex breakdown to occur at a distance $2.5C$ downstream of the trailing edge of the wing. At periods $T_e = 2$ and 1 s of the wing, corresponding to the second and third images of Fig. 3b, the patterns of averaged vorticity $\langle\omega\rangle$ contrast with their counterparts in presence of the impingement edge shown in Fig. 3a. The onset of vortex breakdown is not detectable in the top two images of Fig. 3b. It is barely discernible near the right boundary of the third image, and clearly evident at the left boundary of the fourth image. The presence of the impingement plate, therefore, has a large influence on the location and controllability of vortex breakdown. On the other hand, at the lowest value of excitation $T_e = 0.5$ s, corresponding to the bottom image of Fig. 3b, the onset of vortex breakdown occurs near the left boundary of the image. When this image is compared with the corresponding one of Fig. 3a, it is evident that the averaged vorticity contours are relatively narrow and closely spaced, relative to the case where the edge is present. In fact, this remarkably narrow breakdown bubble in the bottom image of Fig. 3b is substantially narrower than all other breakdown bubbles in presence of an impingement edge, that is, for the case of the stationary edge $T_e = 2$ and 1 s in Fig. 3a. More specifically, compare the images in Figs. 3a and 3b for which the onset of vortex breakdown occurs at the trailing edge of the wing. In Fig. 3a, the appropriate image is at $T_e = 1$ s, and in Fig. 3b, it corresponds to $T_e = 0.5$ s. The presence of the impingement edge, even though it is located well downstream of the onset of vortex breakdown, is associated with a rapid divergence of the vorticity layers along the edge of the breakdown bubble.

Finally, when the images of Figs. 3a and 3b are viewed as a whole, well-defined vorticity layers are present adjacent to the bottom boundary of the images corresponding to the case of the stationary wing and the wing subjected to perturbations at $T_e = 0.5$ s. These layers apparently have no relation to the innermost layers that eventually undergo breakdown. Rather, it is hypothesized that they are associated with a three-dimensional instability of the shear layers separating from the leading edges of the wing.

### Contours of Averaged Velocity in Presence and Absence of Impingement Plate

Contours of constant averaged velocity $\langle V\rangle$ are shown in Figs. 4a and 4b; they correspond to the averaged vorticity $\langle\omega\rangle$ images of Figs. 3a and 3b. In Figs. 4a and 4b, numbers on contours correspond to velocity in millimeter per second; incremental value between the contours is 2.5 mm/s. The nominal angle of attack of the delta wing is $\bar{\alpha} = 24$ deg and the amplitude of the perturbation angle of attack is $\alpha_0 = 1$ deg. The images of Fig. 4a clearly show the retardation and advancement of the onset of vortex breakdown relative to the case of the stationary wing. Moreover, as shown in the first, third, and fourth images of Fig. 4a, corresponding to the stationary wing and the wing at $T_e = 1$ and 0.5 s, very large velocity defects are present in the central region of the vortex breakdown bubble. A much milder defect occurs in the second image corresponding to $T_e = 2$ s.

The corresponding images of Fig. 4b in absence of the impingement plate show the very gradual variations of the velocity along the axis of the vortex, which is indicated by the dashed line. When these velocity contours are compared with those of Fig. 4a, where the impingement plate is present, it is evident that the consequence of the impingement plate is to induce very large gradients of velocity along the axis of the vortex. An exception is the case corresponding to the lowest perturbation period of the wing $T_e = 0.5$ s, represented by the bottom image in Fig. 4b. In this case, it is because the onset of vortex breakdown has been remarkably advanced due to the perturbation. As a consequence, relatively large gradients of velocity along the axis of the vortex are evident, even in absence of the impingement plate.

### Variations of Maximum Averaged Vorticity in Presence of Impingement Plate

A further representation of the consequence of wing perturbations on the vortex structure is shown in Fig. 5. In this case, the impingement plate is deployed, and values of averaged vorticity $\langle\omega\rangle$ are tracked along a locus corresponding to the maximum level of vorticity $\langle\omega\rangle$, as indicated by the black line in the patterns of $\langle\omega\rangle$ shown in the right column of Fig. 5. The corresponding values of $\langle\omega\rangle$ depicted in the left column of Fig. 5 show the substantial influence of wing perturbation. At $T_e = 2$ s, the peak vorticity is substantially

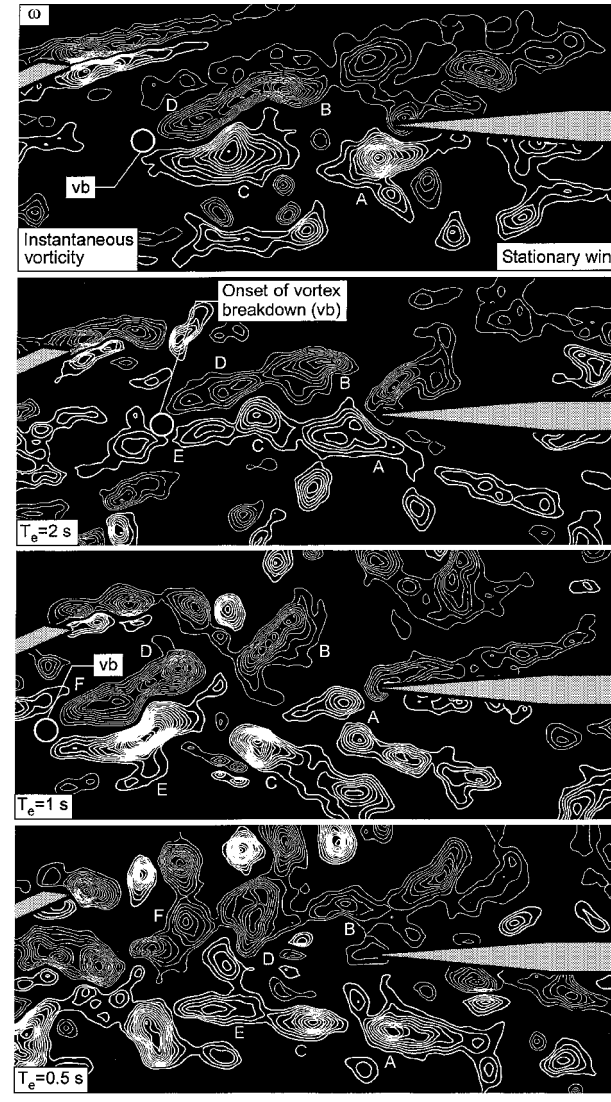


**Fig. 6a Patterns of instantaneous positive (thick line) and negative (thin line) vorticity corresponding to a stationary wing and wing subjected to small-amplitude perturbation at period $T_e$, relative to the period $T_0 = 1.6$ s of the inherent instability of vortex breakdown.**

reduced, and the location of $X/D_v'$, where $X$ is the distance from the left boundary of the image and the vortex diameter and $D_v'$ is a reference diameter measured after the onset of vortex breakdown in the absence of wing perturbation, at which the broad maximum of vorticity occurs is significantly shifted downstream relative to the case of the stationary edge. On the other hand, perturbation at $T_e = 1$ s induces a sharply defined peak in vorticity at a relatively small value of $X/D_v'$. It is followed, however, by a relatively low level of vorticity along the edge of the breakdown bubble. Finally, for the smallest period of excitation $T_e = 0.5$ s, the value of averaged vorticity indicates only a small peak and generally decays by a substantial amount along the separation bubble. Of course, one expects a well-defined peak of vorticity upstream of the left boundary of the image shown in Fig. 4. That is, because vortex breakdown is substantially advanced in the upstream direction, one expects the corresponding peak of vorticity $\langle\omega\rangle$ to occur well upstream of the trailing edge of the wing.

## IV. Instantaneous Structure of Vortex

All of the foregoing averaged features of the onset and development of vortex breakdown are, of course, a consequence of the altered instantaneous structure. Figure 6a provides an overview of instantaneous patterns of vorticity corresponding to the stationary wing and the wing subjected to perturbations $T_e = 2$, 1, and 0.5 s respectively. Viewing these images as a whole, the alteration of location of vortex breakdown is generally in accord with that corresponding to the averaged patterns of vorticity $\langle\omega\rangle$ shown in Fig. 3a. Minimum and incremental values of vorticity are $\omega_{\min} = \pm 1.5$ s$^{-1}$ and $\Delta\omega = 0.5$ s$^{-1}$. Nominal angle of attack of delta wing is $\bar{\alpha} = 24$ deg and the amplitude of the perturbation angle of attack is $\alpha_0 = 1$ deg. To interpret the instantaneous structure in terms of instantaneous clusters of vorticity, analogous clusters indicated as A, B, . . ., F are shown in all images in Fig. 6a. The instantaneous clusters corresponding to the top image, that is, the case of the stationary wing, represent cross-sectional cuts of the spiral mode of inherent vortex breakdown as it encounters the leading edge of the plate. This instability is altered as indicated by the patterns of instantaneous vorticity given in the second image at $T_e = 2$ s. The streamwise distance between, for example, clusters A and C is significantly reduced at $T_e = 2$ s; moreover, the transverse spacing between, for example, vorticity clusters A and B is also reduced. In the third image, corresponding to $T_e = 1$ s, the patterns of vorticity take on a distinctly different form. Vorticity clusters indicated as A, B, and C have become relatively elongated and inclined with respect to the centerline of the breakdown bubble. This overall pattern of instantaneous vorticity is located downstream of high levels of vorticity concentration E, D, and F, due to the upstream advancement of the onset of vortex breakdown. Finally, the image at the bottom of Fig. 6a, corresponding to the lowest period $T_e = 0.5$ s, shows closely spaced, smaller-scale concentrations of vorticity along the edges of the breakdown bubble, in comparison with the case of the stationary edge.

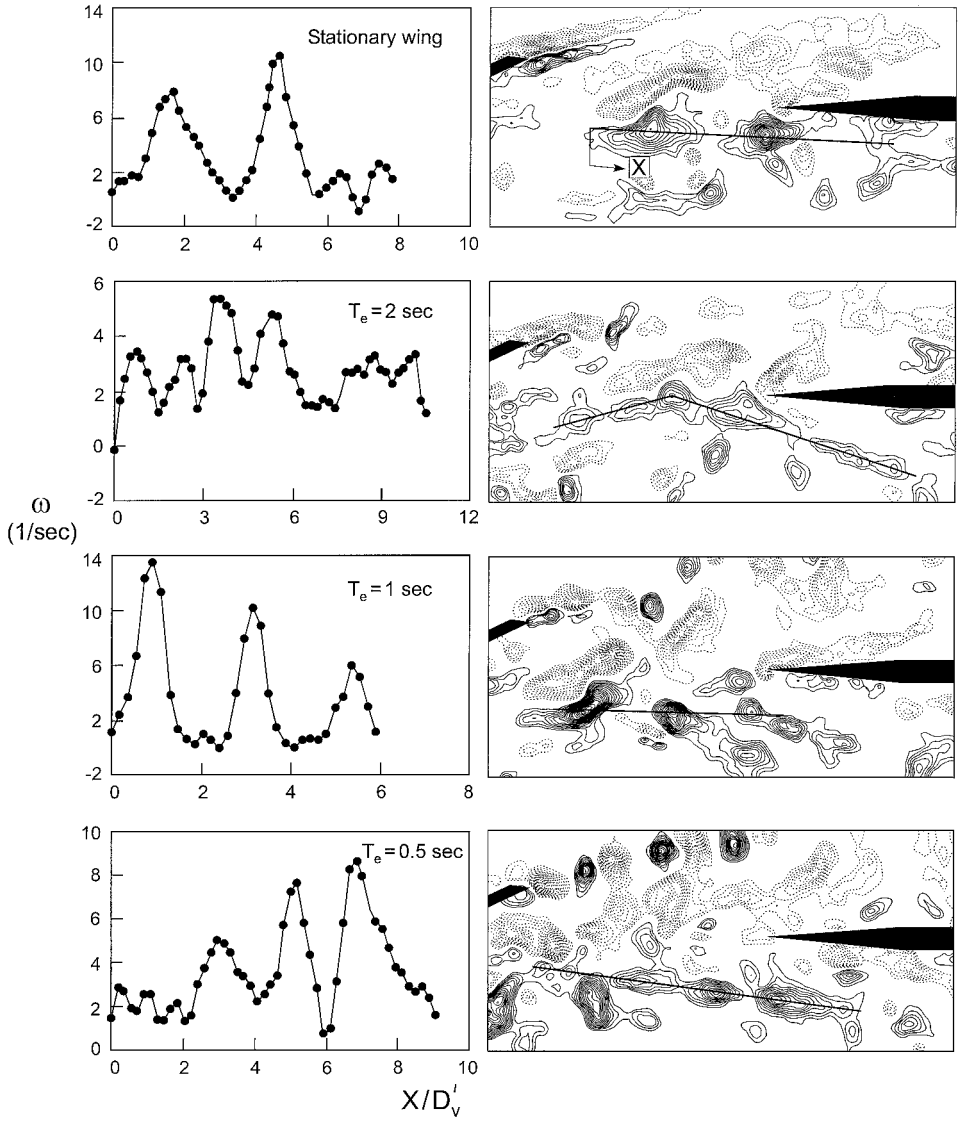


**Fig. 6b Variation of instantaneous vorticity $\omega$ along a line corresponding to maximum positive vorticity for the case of the stationary wing and wing subjected to perturbation of angle of attack at period $T_e$, relative to the period $T_0 = 1.6$ s of the inherent instability of vortex breakdown.**

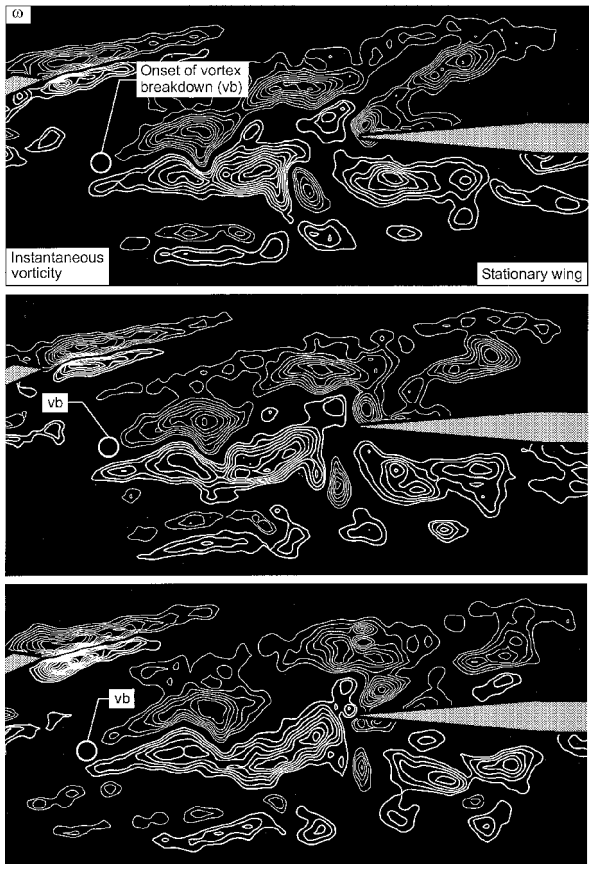


**Fig. 6c Excerpts from cinema sequence showing evolution of patterns of vorticity with time for the case of the stationary delta wing.**

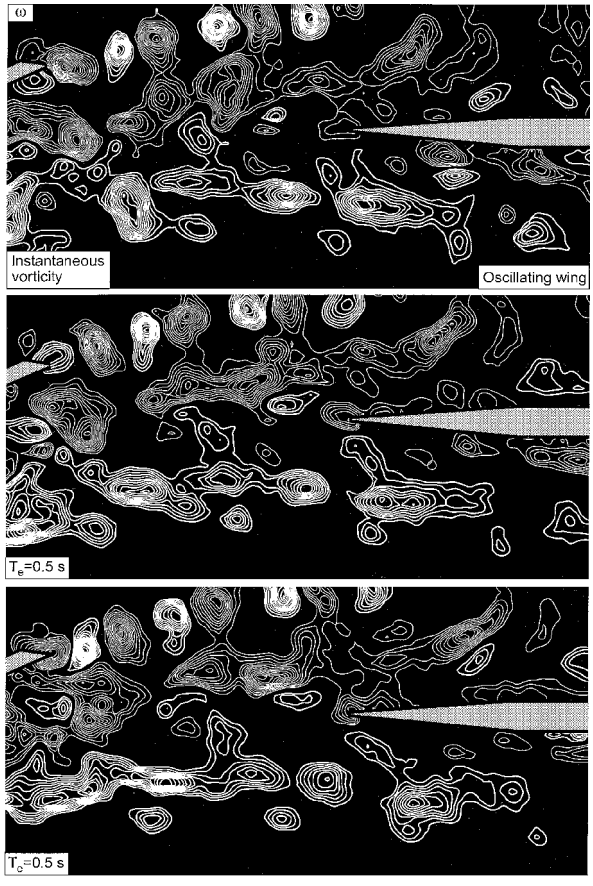


**Fig. 6d Patterns of instantaneous vorticity corresponding to perturbation of delta wing at period $T_e = 0.5$ s, relative to period $T_0 = 1.6$ s of inherent instability of vortex breakdown.**

Important for consideration of buffeting of the plate is the effective wavelength and propagation speed of the instantaneous vortical structures exhibited in Fig. 6a. When the instantaneous images are used therein, it is possible to plot the spatial variation of instantaneous vorticity along the edges of the breakdown bubble. The result is shown in Fig. 6b. In Fig. 6b, coordinate $X$ is the distance from the beginning of the solid line and vortex diameter, and $D_v'$ is a reference diameter measured after the onset of vortex breakdown in the absence of wing perturbation as shown in Fig. 5. At each value of $T_e$, distributions of vorticity shown in the left column of Fig. 6b were evaluated along the thin black lines in the right column of Fig. 6b. First, when the case of the stationary wing is considered, corresponding to the top image of Fig. 6b, the undisturbed, spiral mode of vortex breakdown gives rise to relatively large-scale, widely spaced vorticity concentrations. The corresponding spatial distribution of instantaneous vorticity shown at the left of this image thereby exhibits pronounced peaks having relatively wide spacing. On the other hand, excitation at $T_e = 2$ s induces a series of smaller-scale concentrations of vorticity. Correspondingly, the peaks and the spatial distribution are relatively closely spaced. At the period of excitation $T_e = 1$ s, the patterns of instantaneous vorticity take on a remarkably different form. Although adjacent small-scale concentrations are induced by the excitation, they appear as inclined layers of instantaneous vorticity. As a consequence, a line passing through vorticity contours, such as that designated in Fig. 6b, gives

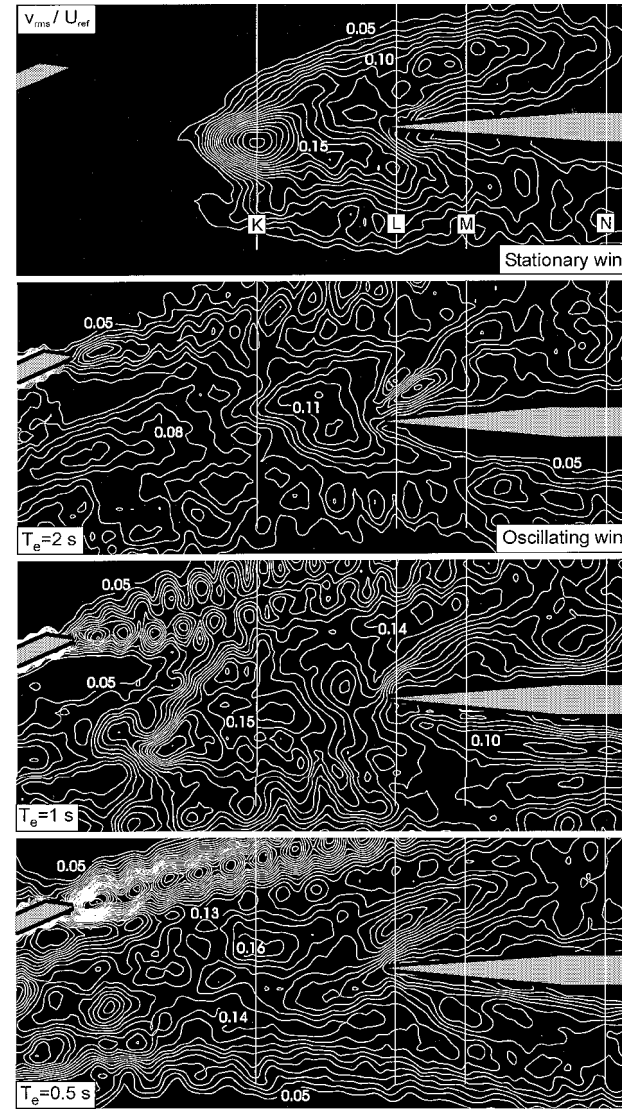


**Fig. 7a Root-mean-square values of transverse velocity fluctuation $v_{rms}$ for the cases of a stationary delta wing and a wing subjected to small-amplitude perturbation of angle of attack.**

rise to relatively widely spaced peaks. At $T_e = 0.5$ s, the small-scale concentrations again become approximately oriented along the indicated line, thereby producing more closely spaced peaks of the spatial distribution of vorticity.

To provide further insight into the space–time evolution of the patterns of instantaneous vorticity, excerpts from cinema sequences are shown in Figs. 6c and 6d. The parameters in Figs. 6c and 6d are the same as for Fig. 6a. Figure 6c corresponds to the case of the stationary wing and Fig. 6d to the wing subjected to perturbations at $T_e = 0.5$ s. In Fig. 6c, the general form of the vorticity concentrations sufficiently far upstream of the impingement plate is preserved. Large changes occur, however, along the upper surface of the plate, where the localized vortex formed from the tip successively interacts with vortical structures originating from the vortex breakdown process. In Fig 6d, the vorticity concentrations exhibit significant distortion, even at locations well upstream of the impingement plate, though the generally small-scale features of individual clusters are identifiable. This small scale is, of course, associated with the low period $T_e$ of excitation of the wing.

## V. Consequence of Vortex Structure on Buffet Flowfield Along Plate Surface

It is well known that an important parameter related to the magnitude of buffeting of aerodynamic surfaces is the transverse velocity fluctuation $v_{\text{rms}}$. It may be viewed as an indicator of the effective fluctuating angle of attack, in accord with the concepts recently outlined by Breitsamter and Laschka[20] and related to previous investigations of the turbulent structure of the flowfield associated with the buffeting, by Breitsamter and Laschka.[18,19] In essence, sufficiently large values of $v_{\text{rms}}$ that are properly correlated along the surface can give rise to a substantial magnitude of buffet loading. Plots of constant contours of root-mean-square transverse velocity fluctuation $v_{\text{rms}}/U_{\text{ref}}$ are indicated in Fig. 7a. $U_{\text{ref}}$ is the reference velocity at a location in the freestream above the trailing edge; its value was 48 mm/s. In Fig. 7a, the wing is perturbed at period $T_e$, relative to the period $T_0 = 1.6$ s of the inherent instability of vortex breakdown. Numbers on the contours correspond to constant values of the dimensionless ratio $v_{\text{rms}}/U_{\text{ref}}$. The minimum and incremental values of the transverse velocity fluctuation are $v_{\text{rms}}/U_{\text{ref}} = 0.05$ and $\Delta v_{\text{rms}}/U_{\text{ref}} = 0.01$. The nominal angle of attack of the delta wing is $\bar{\alpha} = 24$ deg, and the amplitude of the perturbation angle of attack is $\alpha_0 = 1$ deg. Thin vertical lines represent locations at which distributions of $v_{\text{rms}}/U_{\text{ref}}$ are displayed in Fig. 7b. The onset of vortex breakdown, which is clearly designated in the averaged vorticity contours $\langle\omega\rangle$ in Fig. 3a, is associated with concentrated regions of relatively high $v_{\text{rms}}$, evident in images corresponding to the stationary wing and the wing at $T_e = 2$ and 1 s in Fig. 7a. The patterns of velocity fluctuations $v_{\text{rms}}/U_{\text{ref}}$ exhibited in Fig. 7a indicate that the entire flowfield is affected by the perturbation of the delta wing; these patterns indicate the time-averaged consequence of the instantaneous patterns shown in the foregoing image layouts. It is evident in Fig. 7a that substantial distortions are induced within the interior of the vortex, and, moreover, high levels of $v_{\text{rms}}$ occur along the exterior of the vortex, evident by the higher level contours along the bottom edges of the images corresponding to $T_e = 2$, 1, and 0.5 s in Fig. 7a. Finally, note that reasonably high levels are induced in the leading-edge region of the impingement plate for all cases shown in Fig. 7a.

The thin white vertical lines shown in Fig. 7a indicate locations for which vertical distributions of $v_{\text{rms}}/U_{\text{ref}}$ are plotted in Fig. 7b. In Fig. 7b, the wing is perturbed at period $T_e$, relative to period $T_0 = 1.6$ s of the inherent instability of vortex breakdown. The upper left plot of Fig. 7b, which corresponds to line K in Fig. 7a, shows that, for the case of the stationary edge, a peak in $v_{\text{rms}}$ occurs near the plane of symmetry of the breakdown bubble. This peak is generally smoothed out, and the form of the distribution is altered, at locations L, M, and N, where the boundary conditions of the plate surface come into play. Generally speaking, the level of $v_{\text{rms}}$ is substantially reduced for locations K–N at the excitation condition $T_e = 2$ s. At

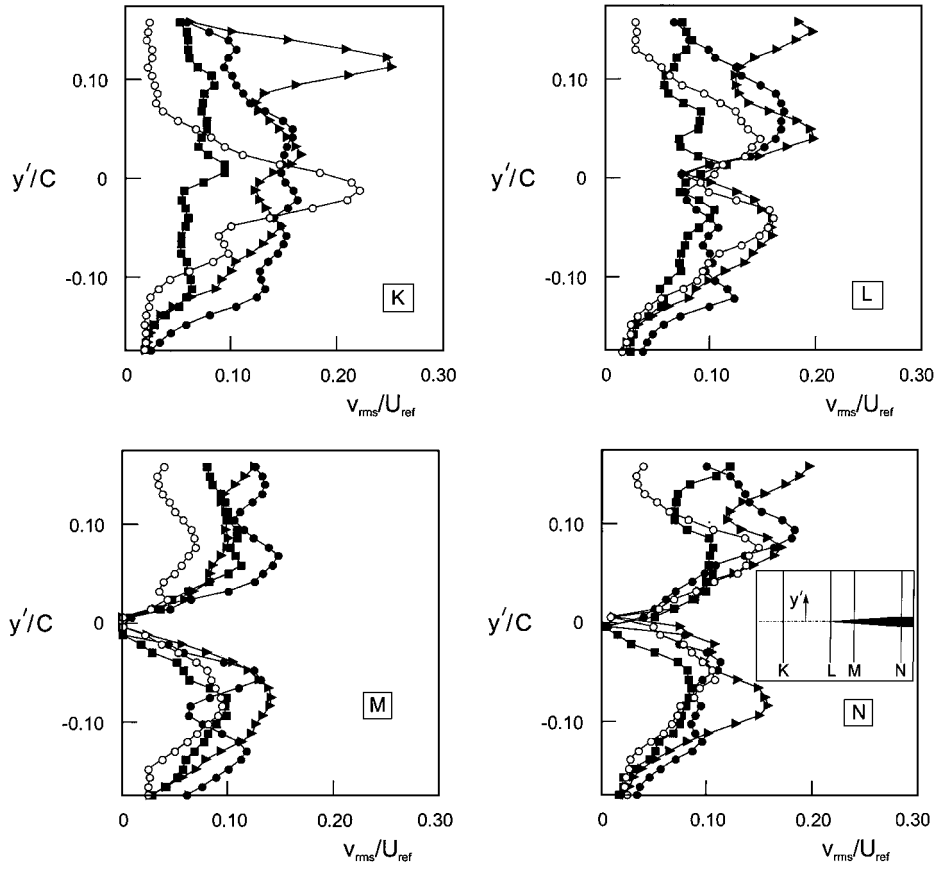


**Fig. 7b Distributions of root-mean-square of transverse velocity fluctuation $v_{\text{rms}}$ normalized by reference velocity $U_{\text{ref}}$ along the vertical lines designated in Fig. 7a: ○, stationary wing; ■, $T_e = 2$ s; ●, $T_e = 1$ s; and ►, $T_e = 0.5$ s.**

the other extreme, the very high level of $v_{rms}$ at the large value of $y'/C$ at location K is due to the induced vortex street from the trailing edge of the wing at $T_e = 0.5$ s. The distributions of the $v_{rms}$ along line L, which is located immediately upstream of the leading edge of the plate, all tend to show local minima at the leading edge. Corresponding distributions along line M all go to zero at the surface of the plate due, of course, to the impermeability condition. Well downstream of the leading edge, corresponding to line N, this same general form of the $v_{rms}$ distributions persists.

## VI. Conclusions

Current interest in deployment of various techniques for controlling leading-edge vortex formation on delta wings that are either stationary or undergoing a maneuver at relatively long timescales have stimulated the present investigation, which simulates key features of leading-edge control by small-amplitude perturbations of a delta wing. The concept is that the very large unsteady pressure gradients at the leading edge induced by small perturbations of the wing will have large consequences, for instantaneous, three-dimensional patterns of vorticity generated from the edge. Indeed, the present investigation shows a substantial influence on both the averaged and instantaneous structure of the leading-edge vortex.

When the wing is perturbed in presence of an impingement plate, either retardation or advancement of the onset of averaged vortex breakdown is attainable. Particularly large values of advancement of vortex breakdown are achieved when the period of oscillation of the edge is approximately equal to the period of inherent vortex breakdown on the corresponding stationary edge. Averaged vorticity contours show that induced vortex breakdown upstream of the edge generally results in rapid divergence of the averaged vorticity layers along the edge of the breakdown bubble. Corresponding distributions of averaged velocity show that, for both the case of the stationary and perturbed wing, large gradients of velocity are generated along the axis of the leading-edge vortex, extending from the leading edge of the breakdown bubble to a location well within the bubble.

On the other hand, when no impingement edge is deployed, the flow patterns are dramatically different. Vortex breakdown generally occurs at locations well downstream of corresponding cases where impingement edge is deployed. Moreover, the transformation of the flow pattern in the region upstream of breakdown is a gradual one, evidenced by the relatively slow variations of velocity along the axis of the vortex. In other words, the consequence of presence of the impingement plate is not simply to induce an earlier onset of breakdown, but also to generate relatively large changes in the averaged structure of the vortex upstream of the breakdown location.

All of these features are related to alteration of patterns of instantaneous vorticity along and within the breakdown bubble. Different classes of patterns have been defined, dependent on the excitation period $T_e$ of the wing. Principal distinctions of these patterns are changes in the streamwise wavelength between clusters of vorticity, as well as the transverse distance between these clusters. A fruitful path for further work would be to relate these observations to wave propagation characteristics along the vortex.

The consequence of buffeting has been interpreted in terms of rms values of transverse velocity fluctuations. The effect of perturbation of the wing at a defined period $T_e$ is shown to produce substantial differences in both the magnitude and shape of distributions of $v_{rms}$ at locations upstream of the impingement plate. At locations well downstream of the leading edge of the plate, however, the form of the vrms distributions is compatible with the zero permeability condition of the plate, and the shape of the $v_{rms}$ distributions is altered accordingly.

## Acknowledgments

The support of the Air Force Office of Scientific Research under Contract F49620-99-1-0011, monitored by Steven Walker, is gratefully acknowledged. One of the authors, Besir Sahin, would like to thank the Scientific and Technical Research Council of Turkey and NATO for their financial support.

## References

[1]Lee, B. H. K., "Vertical Tail Buffeting of Fighter Aircraft," *Progress in Aerospace Sciences*, Vol. 36, No. 3–4, 2000, pp. 193–279.

[2]Wolfe, S., Lin, J.-C., and Rockwell, D., "Buffeting of Fins: An Assessment of Surface Pressure Loading," *AIAA Journal*, Vol. 33, No. 11, 1995, pp. 2232–2235.

[3]Washburn, A. E., Jenkins, L. M., and Ferman, M. A., "Experimental Investigation of Vortex–Fin Interaction," AIAA Paper 93-0050, Jan. 1993.

[4]Bean, D. E., and Wood, N. J., "An Experimental Investigation of Twin Fin Buffeting and Suppression," AIAA Paper 93-0054, Jan. 1993.

[5]Canbazoglu, S., Lin, J.-C., Wolfe, S., and Rockwell, D., "Buffeting of a Fin: Distortion of the Incident Vortex," *AIAA Journal*, Vol. 33, No. 11, 1995, pp. 2144–2150.

[6]Wolfe, S., Lin, J.-C., and Rockwell, D., "Buffeting at the Leading-Edge of a Flat Plate due to a Streamwise Vortex: Flow Structure and Surface Pressure Loading," *Journal of Fluids and Structures*, Vol. 9, No. 4, 1995, pp. 359–370.

[7]Triplett, W. E., "Pressure Measurements on Twin Vertical Tails in Buffeting Flow," *Journal of Aircraft*, Vol. 20, No. 11, 1983, pp. 920–925.

[8]Wentz, W. H., Jr., "Vortex–Fin Interaction on a Fighter Aircraft," *Proceedings of the AIAA 5th Applied Aerodynamics Conference*, AIAA, Washington, DC, 1987, pp. 192–399.

[9]Ferman, N. A., Patel, S. R., Zimmerman, N. H., and Gerstenkorn, G., "A Unified Approach to Buffet Response of Fighter Aircraft Empennage," *AGARD/NATO 70th Structures and Materials Meeting*, 1990, pp. 2-1–2-15.

[10]Zimmerman, N. H., Ferman, M. A., Yurkovich, R. N., and Gerstenkorn, G., "Prediction of Tail Buffet Loads for Design Application," AIAA Paper 89-1378, 1989.

[11]Shah, G. H., "Wind-Tunnel Investigation of Aerodynamic and Tail Buffet Characteristics of Leading-Edge Extension Modifications to the F/A-18," AIAA Paper 91-2889, 1991.

[12]Lee, B. H. K., and Tang, F. C., "Buffet Load Measurements on an F/A-18 Vertical Fin at High Angle-of-Attack," AIAA Paper 92-2127, 1992.

[13]Martin, C. A., and Thompson, D. H., "Scale Model Measurements on Fin Buffet Due to Vortex Bursting on F/A-18," CP-497, AGARD, 1991.

[14]Lee, B. H. K., Brown, D., Tang, F. C., and Plosenski, M., "Flowfield in the Vicinity of an F/A-18 Vertical Fin at High Angle of Attack," *Journal of Aircraft*, Vol. 30, No. 1, 1993, pp. 69–74.

[15]Moses, R. W., and Huttsell, L., "Fin Buffeting Features of an Early F-22 Model," AIAA Paper 2000-1695, 2000.

[16]Luber, W., Becker, J., and Sensburg, O., "The Impact of Dynamic Loads on the Design of Military Aircraft," AGARD-R-815, Sept. 1996, pp. 8-1–8-27.

[17]Ashley, H., Rock, S. M., Digumarthi, R. V., Chaney, K., and Eggers, A. J., Jr., "Active Control for Fin Buffet Alleviation," U.S. Air Force Research Lab., WL-TR-93-3099, Wright–Patterson AFB, OH, Jan. 1994.

[18]Breitsamter, C., and Laschka, B., "Turbulent Flow Structure Associated with Vortex-Induced Fin Buffeting," *Journal of Aircraft*, Vol. 31, No. 4, 1994, pp. 773–781.

[19]Breitsamter, C., and Laschka, B., "Turbulent Flowfield Structure Associated with Fin Buffeting Around a Vortex-Dominated Aircraft Configuration at Sideslip," 19th Congress of the International Council of the Aeronautical Sciences, Vol. 1, Rept. ICAS-94-4.3.2, Sept. 1994, pp. 684–768.

[20]Breitsamter, C., and Laschka, B., "Fin Buffet Pressure Evaluation Based on Measured Flowfield Velocities," *Journal of Aircraft*, Vol. 35, No. 5, 1998, pp. 806–815.

[21]Beutner, T. J., Baust, H. N., and Meyers, J. F., "Doppler Global Velocimetry Measurements of a Vortex–Tail Interaction," *Proceedings of the International Symposium on Flow Visualization*, edited by J. P. Crowder, Begell House, New York, 1995, pp. 418–423.

[22]Mayori, A., and Rockwell, D., "Interaction of a Streamwise Vortex with a Thin Plate: A Source of Turbulent Buffeting," *AIAA Journal*, Vol. 32, No. 10, 1994, pp. 2022–2029.

[23]Canbazoglu, S., Lin, J.-C., Wolfe, S., and Rockwell, D., "Buffeting of a Fin: Streamwise Evolution of Flow Structure," *Journal of Aircraft*, Vol. 33, No. 1, 1995, pp. 185–190.

[24]Rockwell, D., "Vortex–Body Interactions," *Annual Review of Fluid Mechanics*, Vol. 30, 1998, pp. 199–229.

[25]Spedding, G. R., Maxworthy, T., and Rignot, E., "Unsteady Vortex Flows Over Delta Wings," *Proceedings of Second AFOSR Workshop on Unsteady and Separated Flows*, Frank J. Seiler Research Lab., Rept. FJSRL-TR-88-0004, Sept. 1988, pp. 238–288.

[26]Karagounis, T., Maxworthy, T., and Spedding, G. R., "Generation and Control of Separated Vortices Over a Delta Wing by Means of Leading-Edge Flaps," AIAA Paper 89-0997, March 1989.

[27]Gursul, I., Lin, H., and Ho, C.-M., "Vorticity Dynamics of Two-Dimensional and Three-Dimensional Wings in Unsteady Freestream," AIAA Paper 91-0010, Jan. 1991.

[28]Rockwell, D., "Three-Dimensional Flow Structure on Delta Wings at High Angle-of-Attack: Experimental Concepts and Issues," AIAA Paper 93-0550, Jan. 1993.

[29]Shih, Z., Wu, J. M., and Vakili, A. D., "An Investigation of Leading-Edge Vortices on Delta Wings with Jet Blowing," AIAA Paper 87-0330, Jan. 1987.

[30]Visser, K. D., Iwanski, K. T., Nelson, R. C., and Ng, T. T., "Control of Leading-Edge Vortex Breakdown by Blowing," AIAA Paper 88-0504, Jan. 1988.

[31]Wood, M. J., and Roberts, L., "The Control of Vortical Lift on Delta Wings by Tangential Leading-Edge Blowing," AIAA Paper 87-0158, Jan. 1987.

[32]Celik, Z. Z., and Roberts, L., "Aircraft Control at High-Alpha by Tangential Blowing," AIAA Paper 92-0021, Jan. 1992.

[33]Gad-el-Hak, M., and Blackwelder, R. F., "Control of the Discrete Vortices from a Delta Wing," *AIAA Journal*, Vol. 25, No. 8, 1987, pp. 1042–1049.

[34]Gu, W., Robinson, O., and Rockwell, D., "Control of Vortices on a Delta Wing by Leading-Edge Injection," *AIAA Journal*, Vol. 32, No. 7, 1993, pp. 1177–1186.

[35]Findlay, D., Kern, S., and Kwon, O., "Numerical Investigation of the Effect of Blowing on High Angle of Attack Flow Over Delta Wings," AIAA Paper 91-1809, June 1991.

[36]Huttsell, L. J., Tinapple, J. A., and Weyer, R. M., "Investigation of Buffet Loading on a Scaled F-15 Twin Tail Model," AGARD Structures and Materials Panel Workshop, Oct. 1997.

[37]Reynolds, G. A., and Abtahi, A. A., "Instabilities in Leading-Edge Vortex Development," AIAA Paper 87-2424, 1987.

[38]Gursul, I., and Yang, H., "Vortex Breakdown over a Pitching Delta Wing," AIAA Paper 94-0536, Jan. 1994.

[39]Akilli, H., Sahin, B., and Rockwell, D., "Control of Vortex Breakdown by a Transversely-Oriented Wire," *Physics of Fluids*, Vol. 13, No. 2, 2001, pp. 452–463.

[40]Gursul, I., and Xie, W., "Interaction of Vortex Breakdown with an Oscillating Fin," AIAA Paper 2000-0279, Jan. 2000.

[41]Sahin, B., Akilli, H., Lin, J.-C., and Rockwell, D., "Vortex Breakdown-Edge Interaction: Consequence of Edge Oscillations," *AIAA Journal*, Vol. 29, No. 5, 2001, pp. 865–876.

[42]Rockwell, D., Magness, C., Towfighi, J., Akin, O., and Corcoran, T., "High-Image-Density Particle Image Velocimetry Using Laser Scanning Techniques," *Experiments in Fluids*, Vol. 14, 1993, pp. 181–192.